



Seasonal Variations of the Mercury Multiple Isotopic Compositions of Subrural and Urban Aerosols Highlight an Additional Atmospheric Hg⁰ Oxidation Pathway

OPEN ACCESS

David AuYang^{1*}, Jiubin Chen^{1,2*}, Wang Zheng², Yunchao Lang², Yina Wang³, Zhongwei Wang¹, Yuanyuan Zhang¹, Yulong Liu¹, Ke Zhang², Hongming Cai², Wei Yuan² and David Widory⁴

Edited by:

Adrien Mestrot,

University of Bern, Switzerland

Reviewed by:

Carl Mitchell,

University of Toronto Scarborough,
Canada

Rute Isabel Cesário,

University of Lisbon, Portugal

*Correspondence:

David AuYang

auyangdavid@gmail.com

Jiubin Chen

jbchen@tju.edu.cn

Specialty section:

This article was submitted to

Biogeochemical Dynamics,

a section of the journal

Frontiers in Environmental Science

Received: 09 September 2021

Accepted: 07 December 2021

Published: 17 January 2022

Citation:

AuYang D, Chen J, Zheng W, Lang Y, Wang Y, Wang Z, Zhang Y, Liu Y, Zhang K, Cai H, Yuan W and Widory D (2022) Seasonal Variations of the Mercury Multiple Isotopic Compositions of Subrural and Urban Aerosols Highlight an Additional Atmospheric Hg⁰ Oxidation Pathway. *Front. Environ. Sci.* 9:773327. doi: 10.3389/fenvs.2021.773327

¹State Key Laboratory of Environmental Geochemistry, Institute of Geochemistry, Chinese Academy of Sciences, Guiyang, China, ²Institute of Surface-Earth System Science, Tianjin University, Tianjin, China, ³Qiushi Honors College, Tianjin University, Tianjin, China, ⁴GEOTOP/ Université du Québec à Montréal, Montréal, QC, Canada

The mechanisms triggering the large variations in the mercury (Hg) multiple isotopic compositions of atmospheric particle-bound Hg worldwide still remain unclear. The comparison of Hg isotopic compositions in aerosols collected in urban and rural areas may help distinguish the effects of natural processes from those of anthropogenic inputs. We thus investigated the Hg isotopic compositions of PM₁₀ aerosols collected seasonally during 2015 at two monitoring stations on Montreal Island, one located downtown and the other in its westernmost subrural part, barely impacted by the city anthropogenic emissions. Our results show that, while Hg isotopic compositions present no seasonality at the urban station, possibly due to constant anthropogenic emissions, the subrural samples display clear seasonal variations, with higher $\Delta^{199}\text{Hg}$ and $\Delta^{200}\text{Hg}$ values (up to 0.77 and 0.12‰, respectively) during summer and close to 0‰ during the rest of the year, that cannot solely be explained by anthropogenic primary emissions. Besides, $\Delta^{200}\text{Hg}$ measured in the subrural aerosols display a positive correlation with O₃ suggesting the implication of secondary processes involving ozone. We propose that the significant summer shift in the multiple Hg isotopic compositions may reflect a transition in the corresponding Hg⁰ oxidation pathway, from halogens-triggered to ozone-dominated reactions. Still, this hypothesis needs to be further tested. Nevertheless, it demonstrates that Hg isotopes are effective at characterizing secondary processes that control its atmospheric budget, even at a local scale (i.e., urban vs subrural) and could thus be used to better constrain its atmospheric chemistry in various environments.

Keywords: mass-independent fractionation (MIF), mercury isotope, aerosols, oxidation, ozone

1 INTRODUCTION

Mercury (Hg) is a toxic element that has the ability to be remobilized at large scales in the atmosphere following successive oxidation and reduction reactions. Gaseous elemental mercury (Hg^0), the dominant Hg form in the atmosphere, is relatively stable and has a relatively long lifetime of 0.5 to 1 year that allows it to be transported over long distances worldwide (Selin 2009). Hg^0 can be oxidized into reactive mercury (Hg^{II}) through several possible pathways [e.g., Si et al. (2018)]. Hg^{II} can then be incorporated into particles by adsorption [see Si et al. (2018)], forming particles bound mercury (PBM). Once deposited, Hg^{II} may be transformed into methylmercury in aquatic system (MeHg^+) that can then bioaccumulate in living aquatic organisms and ultimately impact human health (Sunderland 2007). This emphasizes the need to better constrain the different oxidation pathways that Hg^0 undergoes in the atmosphere. However, the dominant oxidation and reduction mechanisms controlling atmospheric Hg, and their respective reaction rates, are still subject to debate (Saiz-Lopez et al., 2018) as discrepancies between the observed and modelled residence time and spatiotemporal distribution of Hg^0 remain (Horowitz et al., 2017).

The study of the Hg isotopic systematics may help distinguish and identify the different oxidation pathways involved. Hg possesses seven stable isotopes, ^{196}Hg , ^{198}Hg , ^{199}Hg , ^{200}Hg , ^{201}Hg , ^{202}Hg , and ^{204}Hg with respective abundances of 0.15, 9.97, 16.87, 23.10, 13.18, 29.86 and 6.87%. Previous studies showed the Hg multi-isotopic compositions in particular the use of Mass dependent Fractionation and Mass Independent Fractionation (MDF and MIF respectively, see Methods for definitions) as powerful tracers of Hg sources, allowing the characterization of the processes that control Hg budget in the atmosphere (Rolison et al., 2013; Das et al., 2016; Fu et al., 2016; Yu et al., 2016; Zheng et al., 2016; Xu et al., 2017; Fu et al., 2019; Huang et al., 2019; Xu et al., 2019; Zhang et al., 2020). Previous studies have shown that aerosols collected in various regions are characterized by $\Delta^{199}\text{Hg}$ varying from -1.50 to 1.50% , $\Delta^{200}\text{Hg}$ varying from -0.20 to 1.20% and $\Delta^{201}\text{Hg}$ varying from -1.50 to 1.50% (Rolison et al., 2013; Das et al., 2016; Yu et al., 2016; Xu et al., 2017; Fu et al., 2019; Huang et al., 2019; Xu et al., 2019). Mass-Independent Fractionation of odd Hg isotopes (odd-MIF; i.e., $\Delta^{199}\text{Hg}$ and $\Delta^{201}\text{Hg}$) are mainly caused by the magnetic isotope effect (MIE) and the nuclear volume effects (NVE) (Bergquist et al., 2007; Buchachenko 2013; Cai et al., 2016) and are mainly produced during photochemical reduction of Hg^{2+} , MeHg photo-demethylation, abiotic dark reduction and liquid-vapor evaporation (Bergquist et al., 2007; Estrade et al., 2009; Zheng et al., 2009; Zheng et al., 2010). These processes produce specific $\Delta^{199}\text{Hg}/\Delta^{201}\text{Hg}$ ratios, rendering this parameter a unique tool for characterizing the biogeochemical processes that Hg undergoes in the environment (Bergquist et al., 2007; Zheng et al., 2009; Sherman et al., 2010; Sun et al., 2016). On the other hand, the mechanisms triggering even-MIF (i.e., $\Delta^{200}\text{Hg}$ and $\Delta^{204}\text{Hg}$) that were reported in many atmosphere-related studies (Sherman et al., 2010; Chen et al., 2012; Wang et al., 2015; Yuan et al., 2015; Yuan et al., 2018) remain unknown,

although some suggested that it may be related to the photochemical oxidation of elemental Hg^0 in the tropopause (Chen et al., 2012) or to specific reactions (e.g., self shielding effect in compact fluorescent lamp (Mead et al., 2013) or a molecular magnetic isotope effect during Hg^{II} photoreduction (Fu et al., 2021)). More recently, Sun et al. (2016) proposed that the oxidation of Hg^0 by halogen atoms also produces both odd- and even-MIF, suggesting the potential for oxidation reactions to trigger MIF of Hg isotopes, especially in atmospheric samples such as aerosols.

It must be noted that most of the reported odd and even-MIF measured in aerosols cannot be fully explained by these processes, and thus remain subject to debate. Atmospheric PBM results from 1) direct emissions of anthropogenic sources, whose contributions may account for 40% of the total PBM in polluted areas (Xiao et al., 1991) and/or 2) secondary atmospheric processes like a series of Hg oxidation by halogen atom and/or by OH followed by Hg photoreduction (Holmes et al., 2010; Subir et al., 2012; Horowitz et al., 2017). However, to our knowledge, only limited studies focused on the Hg multiple isotopic compositions of aerosols collected in moderately polluted or rural environments (Rolison et al., 2013; Yu et al., 2016; Fu et al., 2019) where the influence of those secondary processes (Holmes et al., 2010; Horowitz et al., 2017) remains rarely investigated (Fu et al., 2019; Huang et al., 2019). In particular, no study, to our knowledge, has yet been undertaken to compare the Hg isotopic compositions of aerosols collected in urban and sub-rural areas from a single region, although this should help distinguish the effects of natural processes from those of anthropogenic inputs. In this study, we investigated the Hg multiple isotopic compositions measured in aerosols collected over 1 year (i.e., covering the four seasons) at two different stations in Montreal (Canada), an urban and a sub-rural station, in order to constrain the respective impacts of natural and anthropogenic processes on the final Hg isotopic compositions, and to characterize potential mechanisms triggering their corresponding MIF.

2 MATERIALS AND METHODS

2.1 Sampling Sites

Montreal is considered a relatively lowly air-contaminated city, with an average annual PM_{10} (particles with an aerodynamical diameter $<10\ \mu\text{m}$) concentration of $16\ \mu\text{g m}^{-3}$ (World Health Organization 2016), lower than the $20\ \mu\text{g m}^{-3}$ guidelines set by the WHO. Still, the city exhibits local variations at several monitoring stations and records discrete episodes of air pollutions with concentrations exceeding the mean $50\ \mu\text{g m}^{-3}$ 24-h guidelines (Boulet and Melancon, 2012; Boulet and Melancon, 2013). PM_{10} aerosols were sampled over a 1-year period in 2015 by the RSQA (Réseau de Surveillance de la Qualité de l'Air) in Montreal ($45^\circ\text{N } 73^\circ\text{W}$, Canada) and its vicinity, in collaboration with the Ville de Montréal. Two monitoring stations (13 and 98) disseminated onto Montreal Island were selected for their specific environmental conditions (**Figure 1**). Station 13, referred as “Drummond,” is located downtown and

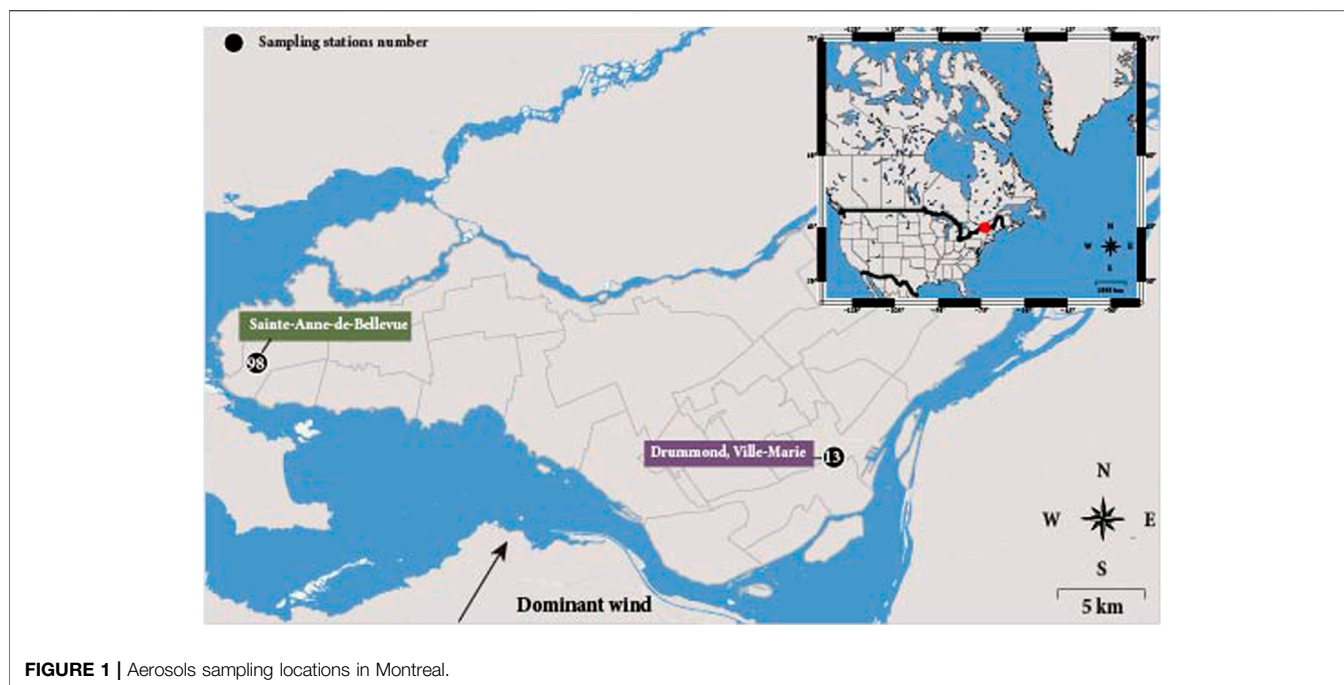


FIGURE 1 | Aerosols sampling locations in Montreal.

represents the urban background, whereas Station 98 referred as “Sainte-Anne de Bellevue” is located at the westernmost end of the island, in a semi-rural environment under dominant southwest-northeast blowing winds, and thus represents a station less impacted by local anthropogenic atmospheric emissions (Boulet and Melancon, 2012). Station 13 is thus expected to collect aerosols of both local and more distant sources, i.e., emitted locally and brought to Montreal, compared to station 98 where aerosols are expected to mostly come from outside the city. Our sampling strategy was thus designed to allow comparing a station mostly affected by local anthropogenic emissions to a station where aerosols are expected to have a remote origin (i.e., aerosols transported to Montreal). At this second station, aerosols are expected to at least partially derive from atmospheric secondary processes. In parallel, major pollutant gases, including ozone (O_3), sulfur dioxide (SO_2), nitrogen dioxide (NO_2), as well as $PM_{2.5}$ hourly concentrations were continuously acquired from the Réseau de Surveillance de la Qualité de l’Air (RSQA) for both stations (<http://ville.montreal.qc.ca/>, last access: 02 January 2020). We calculated daily mean concentrations for each compound in order to fit with the 24 h sampling period of the aerosols.

PM_{10} samples and blank samples were also weekly collected by the RSQA on pre-combusted quartz filters using a high volume PM_{10} size selective inlet, with an average flow of $1.13 \text{ m}^3 \text{ min}^{-1}$ for a period of 24 h (pumped air volume of $\sim 1627 \text{ m}^3$ per filter). Within the sample set, four samples were selected and analyzed each month during an entire year, with two samples collected at station 13 and two others at station 98. Samples selected at each station were collected on the same day during the first 2 weeks of each month. Blank filters were analyzed randomly for each site, and yielded Hg concentrations under the analytical detection limit ($<0.1 \text{ ppb}$).

2.2 Elemental Concentration Measurement

Concentrations of selected soluble inorganic species (Na^{2+} , K^+ , Ca^{2+} , Mg^{2+} , NO_3^- , SO_4^{2-} , Cl^-) were measured using a Dionex ICS-90 Ion Chromatography system, after extraction from a $3 \text{ cm} \times 3 \text{ cm}$ filter piece with 30 ml of Milli-Q water, following the method described by Paris et al. (2010). Detection limits for these ion species were usually in the order of $5 \mu\text{g L}^{-1}$, i.e., 0.1 ng m^{-3} considering our sampling and extraction protocols. Hg concentrations were measured by cold vapor atomic fluorescence spectroscopy (CVAFS, Tekran 2500) after reducing an aliquot of the pre-concentrated Hg^{II} (i.e., acid trap solution) into Hg^0 using $SnCl_2$. The Hg^0 was then collected on a gold-coated bead trap and analyzed by CVAFS (Huang et al., 2015).

2.3 Hg Multiple Isotopic Compositions Measurement

Aerosol filters were combusted using the dual-stage protocol described in Huang et al. (2015) to concentrate Hg. Briefly, each filter was introduced into a quartz tube that then underwent two successive combustions first at 950°C , followed by a combustion at 1000°C for a total time of 3.5 h to decompose the Hg^{II} present under the form of Hg_p into vapor Hg^0 (Sun et al., 2013). The combustion products, Hg^0 (and other compounds if any), were purged using Hg-free O_2 , and bubbled through a 5 ml HNO_3 -HCl- H_2O mixture (2:4:9) acid trap (Sun et al., 2013; Huang et al., 2015). The generated solution was then transferred into a pre-cleaned glass bottle. $50 \mu\text{l}$ of 0.2 M BrCl were then added to fully convert Hg^0 into Hg^{II} .

Hg^{II} was then converted back into Hg^0 by reacting with $SnCl_2$ and injected into a multi-collector inductively coupled plasma mass spectrometer (MC-ICPMS; Neptune plus) simultaneously

TABLE 1 | Mercury multi-isotopic compositions and major anions and cations measured in aerosol samples collected in Montreal. Corresponding O₃ concentrations, measured at station 13, are also reported.

Station 13															
Date	Hg	δ ²⁰² Hg	Δ ²⁰¹ Hg	Δ ²⁰⁰ Hg	Δ ¹⁹⁹ Hg	Cl ⁻	NO ₃ ⁻	SO ₄ ²⁻	Ca ²⁺	K ⁺	Mg ²⁺	Na ²⁺	O ₃	NO	NO ₂
	ng.m ⁻³	± 0.1‰ (1σ)	± 0.02‰ (1σ)	± 0.02‰ (1σ)	± 0.01‰ (1σ)	ng.m ⁻³	ng.m ⁻³	ng.m ⁻³	ng.m ⁻³	ng.m ⁻³	ng.m ⁻³	ng.m ⁻³	ppb	ppb	ppb
12-01-15	35.7	-4.0	0.01	0.04	0.18	6.35	11.04	7.21	9.61	0.68	0.14	12.52	13.1	14.7	23.6
17-01-15	1481.7	-2.9	-0.06	0.04	-0.02	7.95	16.48	10.31	7.26	1.06	0.28	14.17	20.9	6.7	16.8
17-02-15	240.3	-2.3	0.02	0.04	0.03	43.19	14.03	10.09	6.72	1.18	0.32	38.52	10.6	24.0	30.1
23-02-15	3289.2	-2.2	-0.06	0.00	0.00	10.22	3.80	7.53	4.71	0.64	0.19	11.36	18.9	10.1	12.7
01-03-15	419.6	-2.5	-0.05	0.01	-0.01	36.11	16.17	11.68	7.09	1.12	0.25	35.67	28.9	3.7	21.7
07-03-15	93.4	-2.4	-0.02	0.07	-0.01	8.09	20.65	13.78	7.45	0.97	0.28	17.73	34.1	4.3	18.0
06-04-15	1660.5	-2.0	-0.03	-0.01	0.01	5.00	7.45	7.82	6.86	0.55	0.15	8.47	26.3	4.8	16.2
12-04-15	789.7	-3.0	0.06	0.05	0.09	0.67	6.20	5.83	6.68	0.47	0.16	4.50	36.2	2.4	8.8
06-05-15	263.4	-2.1	0.04	0.04	0.11	0.97	5.32	5.31	6.72	0.63	0.22	4.22	25.8	12.1	18.2
12-05-15	378.6	-1.6	0.03	-0.04	0.03	0.38	4.82	6.93	4.88	0.56	0.13	4.77	21.2	8.8	12.0
05-06-15	311.1	-2.5	-0.01	0.02	0.07	0.42	6.04	5.42	8.28	0.60	0.20	3.81	20.7	8.2	17.6
11-06-15	773.6	-1.6	-0.01	0.02	-0.02	0.35	2.09	5.01	6.04	0.73	0.18	4.09	23.5	7.1	11.0
05-07-15	22.1	-1.3	0.09	0.03	0.18	0.41	3.59	3.86	4.60	0.69	0.12	4.13	23.8	2.4	7.7
11-07-15	74.6	-2.2	0.32	0.04	0.32	0.23	3.29	4.11	5.34	0.72	0.14	4.02	31.9	3.3	9.2
04-08-15	869.6	-2.9	-0.01	0.04	0.02	0.17	3.10	3.55	3.44	0.56	0.13	3.46	30.1	6.2	10.5
10-08-15	1454.0	-2.7	0.01	-0.01	0.02	0.70	5.09	5.56	8.30	0.57	0.38	3.78	17.1	8.3	12.9
03-09-15	231.5	-3.1	0.02	0.03	0.08	0.50	3.69	6.86	6.86	0.65	0.32	4.56	19.6	7.5	12.7
09-09-15	381.2	-3.2	0.02	0.02	0.02	0.43	4.13	10.53	8.77	1.02	0.38	5.78	22.0	8.0	14.8
03-10-15	297.3	-3.1	0.00	0.03	0.11	0.80	3.14	2.88	4.18	0.38	0.13	2.87	15.9	4.3	5.8
09-10-15	134.7	-2.6	0.03	0.00	0.16	0.30	5.95	4.89	4.86	0.56	0.14	3.93	8.0	16.8	13.8
02-11-15	120.9	-3.4	-0.02	0.02	0.13	0.38	1.85	3.39	2.14	0.35	0.05	2.89	9.3	21.3	17.4
08-11-15	97.1	-3.2	0.01	0.04	0.12	0.17	1.02	2.76	3.76	0.41	0.09	3.29	20.5	3.1	7.0
02-12-15	54.6	-3.1	0.02	0.00	0.12	0.32	3.01	6.20	2.39	0.58	0.084	4.20	3.5	28.9	22.2
08-12-15	60.8	-2.4	0.03	0.05	0.10	1.06	3.35	6.02	5.33	0.62	0.23	4.71	8.2	14.1	18.6

with Tl, which was used as an internal standard to correct for the instrumental mass bias (Blum et al., 2007; Yin et al., 2016). A high concentration of Tl (20 ppb) was injected with each sample to prevent the formation of Hg hybrids during the analysis (Yin et al., 2016). The faraday cups were positioned to collect ¹⁹⁸Hg (L3), ¹⁹⁹Hg (L2), ²⁰⁰Hg (L1), ²⁰¹Hg (C), ²⁰²Hg (H1), ²⁰³Tl (H2), and ²⁰⁵Tl (H3). Hg multi-isotopic compositions were then determined by standard bracketing using the Hg NIST 3133 international standard. The Hg isotopic compositions are expressed as (Blum et al., 2007):

$$\delta^x \text{Hg} = \left[\frac{({}^x\text{Hg}/{}^{198}\text{Hg})_{\text{sample}}}{({}^x\text{Hg}/{}^{198}\text{Hg})_{\text{std}}} - 1 \right] \times 1000 \quad (1)$$

Where x = 199, 200, 201, 202, 204, and “std” is the NIST SRM 3133 Hg international standard. In general, the Hg multiple isotopic ratios are related to each other according to their mass, called the mass-dependent fractionation (MDF), which is expressed as follows (Young et al., 2002; Dauphas et al., 2016):

$${}^y\alpha = ({}^{202}\alpha)^{y\beta} \quad (2)$$

Where ^yα is either ¹⁹⁹α, ²⁰⁰α, ²⁰¹α or ²⁰⁴α and ^yβ is either ¹⁹⁹β, ²⁰⁰β, ²⁰¹β or ²⁰⁴β. The ^{3y}β -exponent describes the relative fractionation of ^yHg/¹⁹⁸Hg compared to ²⁰²Hg/¹⁹⁸Hg where ¹⁹⁹β, ²⁰⁰β, ²⁰¹β and ²⁰⁴β-values are respectively 0.252, 0.502, 0.752 and 1.493 under equilibrium (Blum et al., 2007). The α-notation corresponds to the different isotopic fractionation factors between ¹⁹⁸Hg and any

of the other isotopes. For the oxidation of Hg⁰ into Hg^{II}, α is defined as follows (expressed here for the oxidation of Hg⁰ into Hg^{II}):

$${}^x\alpha_{\text{HgII-Hg0}} = \frac{({}^x\text{Hg}/{}^{198}\text{Hg})_{\text{HgII}}}{({}^x\text{Hg}/{}^{198}\text{Hg})_{\text{Hg0}}} = \frac{\delta^x\text{Hg}_{\text{HgII}}/1000 + 1}{\delta^x\text{Hg}_{\text{Hg0}}/1000 + 1}$$

Any deviation of the Hg isotopic ratios from MDF is defined as the mass-independent fractionation (MIF) and is represented by the “capital delta” notation (Δ^xHg, in ‰) defined following (Farquhar and Wing, 2003; Blum et al., 2007):

$$\Delta^{199}\text{Hg} = 1000 \times \left[\left(\ln \left(\left\{ \delta^{199}\text{Hg}/1000 \right\} + 1 \right) \right) - 0.2520 \left(\ln \left(\left\{ \delta^{202}\text{Hg}/1000 \right\} + 1 \right) \right) \right] \quad (3)$$

$$\Delta^{200}\text{Hg} = 1000 \times \left[\left(\ln \left(\left\{ \delta^{200}\text{Hg}/1000 \right\} + 1 \right) \right) - 0.5024 \left(\ln \left(\left\{ \delta^{202}\text{Hg}/1000 \right\} + 1 \right) \right) \right] \quad (4)$$

$$\Delta^{201}\text{Hg} = 1000 \times \left[\left(\ln \left(\left\{ \delta^{200}\text{Hg}/1000 \right\} + 1 \right) \right) - 0.7520 \left(\ln \left(\left\{ \delta^{202}\text{Hg}/1000 \right\} + 1 \right) \right) \right] \quad (5)$$

TABLE 2 | Mercury multi-isotopic compositions and major anions and cations measured in aerosol samples collected in Montreal. Corresponding O₃ concentrations, measured at station 98, are also reported.

Date	Station 98														
	Hg	$\delta^{202}\text{Hg}$	$\Delta^{201}\text{Hg}$	$\Delta^{200}\text{Hg}$	$\Delta^{199}\text{Hg}$	Cl ⁻	NO ₃ ⁻	SO ₄ ²⁻	Ca ²⁺	K ⁺	Mg ²⁺	Na ²⁺	O ₃	NO	NO ₂
	ng.m ⁻³	± 0.1‰ (1σ)	± 0.02‰ (1σ)	± 0.02‰ (1σ)	± 0.01‰ (1σ)	ng.m ⁻³	ng.m ⁻³	ng.m ⁻³	ng.m ⁻³	ng.m ⁻³	ng.m ⁻³	ng.m ⁻³	ppb	ppb	ppb
12-01-15	27.6	-2.909	-0.05	0.04	-0.02	8.21	8.95	7.26	3.55	0.58	0.07	12.29	23.4	1.4	9.2
17-01-15	92.7	-2.199	0.11	0.08	0.02	7.95	12.46	7.25	4.87	0.99	0.24	13.95	28.8	0.4	6.0
17-02-15	118.6	-1.704	0.11	0.02	0.18	53.31	14.35	9.51	5.95	1.04	0.23	46.13	13.1	21.2	33.8
23-02-15	1019.9	-2.510	-0.03	0.02	0.00	13.91	2.76	5.87	3.60	0.60	0.18	13.94	24.7	0.4	4.9
01-03-15	63.5	-2.112	-0.09	0.07	-0.07	18.70	17.43	9.31	5.50	0.98	0.20	24.19	36.9	1.7	10.8
07-03-15	140.1	-2.144	-0.08	0.05	-0.04	0.51	21.86	13.44	5.71	0.87	0.30	14.83	43.8	0.3	5.7
06-04-15	239.1	-2.567	0.04	0.03	0.05	0.93	9.92	5.35	7.75	0.51	0.14	5.99	29.1	1.0	7.1
12-04-15	677.5	-2.057	-0.06	-0.01	-0.03	0.15	5.19	6.53	4.04	0.50	0.10	5.32	40.0	0.2	2.2
06-05-15	14.7	-3.389	0.16	0.02	0.37	0.47	5.97	4.50	4.44	0.84	0.21	5.87	31.9	2.6	7.3
12-05-15	1847.5	-1.560	-0.06	0.01	0.05	0.24	8.45	9.01	4.14	0.59	0.10	6.67	25.9	0.8	4.2
05-06-15	390.4	-2.100	-0.10	-0.04	-0.01	0.20	5.47	6.40	5.20	0.75	0.22	5.57	25.8	0.9	5.8
11-06-15	42.5	-2.568	0.10	0.04	0.16	0.18	3.02	4.03	4.05	0.73	0.13	4.57	29.1	0.1	2.7
05-07-15	86.5	-3.764	0.24	0.06	0.39	0.28	3.16	4.82	3.48	0.71	0.12	5.03	29.1	0.1	3.0
11-07-15	44.2	-1.215	0.68	0.12	0.77	0.24	13.84	3.91	3.38	0.63	0.08	3.78	35.1	0.0	2.8
04-08-15	315.9	-2.510	0.01	0.04	0.01	0.14	3.40	2.43	2.58	0.37	0.06	2.78	26.5	0.2	2.6
10-08-15	79.3	-2.423	0.31	0.07	0.19	0.33	6.64	4.17	4.76	0.62	0.17	3.92	30.4	1.8	4.3
03-09-15	100.1	-3.085	0.35	0.07	0.77	0.16	4.26	7.04	4.97	0.70	0.16	5.26	27.6	0.2	4.2
09-09-15	78.4	-2.637	0.04	0.02	0.12	1.99	4.15	9.36	5.14	0.72	0.18	5.58	31.1	0.1	3.5
03-10-15	30.3	-2.894	0.01	0.01	0.14	0.40	1.85	2.69	3.13	0.32	0.09	2.59	19.4	0.1	1.3
09-10-15	84.0	-2.961	0.01	-0.01	0.11	0.24	2.64	4.78	2.66	0.39	0.08	3.33	13.8	0.3	4.5
08-11-15	69.3	-2.740	-0.03	0.00	0.11	0.13	1.26	1.33	0.59	0.30	0.02	2.51	17.1	5.8	4.4
14-11-15	39.9	-2.555	0.01	0.01	0.08	0.12	1.04	2.21	0.61	0.20	0.02	1.55	25.4	0.0	0.8
02-12-15	90.6	-2.566	0.00	-0.02	0.07	0.11	3.27	3.57	0.62	0.44	0.04	3.50	4.8	1.5	9.4
08-12-15	77.4	-2.074	-0.08	-0.02	0.02	0.59	4.18	5.25	4.74	0.42	0.19	3.43	11.3	1.8	12.3

The NIST 3177 standard was also regularly analyzed with concentrations matching those of the aerosol samples (i.e., 2 ppb) to control the instrument stability and to guarantee the measurement quality (Geng et al., 2018). Repeated analyses ($n = 22$) of the NIST 3177 standard yielded $\delta^{202}\text{Hg} = -0.52 \pm 0.03\text{‰}$ (2σ), $\Delta^{199}\text{Hg} = -0.02 \pm 0.05\text{‰}$ (2σ), $\Delta^{200}\text{Hg} = 0.01 \pm 0.03\text{‰}$ (2σ), $\Delta^{201}\text{Hg} = -0.01 \pm 0.02\text{‰}$ (2σ) relative to NIST 3133, consistent with previous reported values (Wang et al., 2015; Chen et al., 2016; Sun et al., 2016; Yuan et al., 2018; Fu et al., 2019; Zhang et al., 2020). A Chinese loamy sand CRM024, used as a second certified reference material, with a Hg concentration of 0.71 ppm was also analyzed ($n = 8$). The result yielded a recovery of $104 \pm 7\%$ after pre-concentration by dual-stage combustion, and $\delta^{202}\text{Hg} = -1.43 \pm 0.08\text{‰}$ (2σ), $\Delta^{199}\text{Hg} = 0.03 \pm 0.02\text{‰}$ (2σ), $\Delta^{200}\text{Hg} = -0.00 \pm 0.02\text{‰}$ (2σ), $\Delta^{201}\text{Hg} = 0.00 \pm 0.01\text{‰}$ (2σ), in good agreement with the Hg isotopic compositions reported by Huang et al. (2015).

2.4 HYSPLIT Back-Trajectories Modelling and Statistical Methods

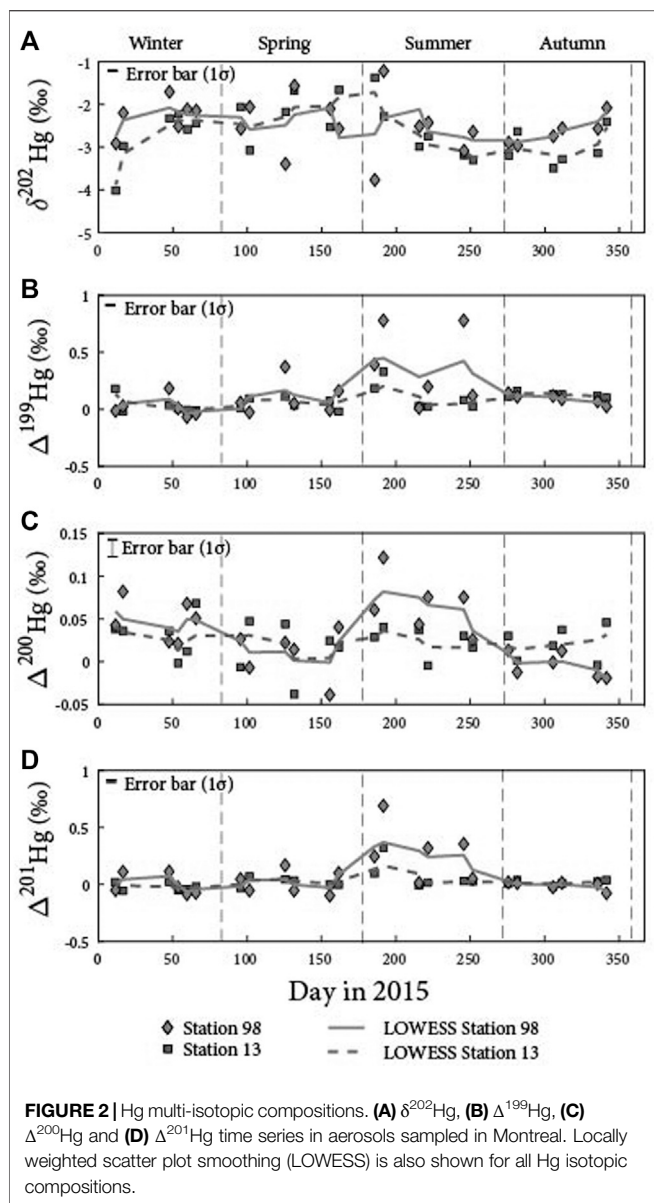
To investigate potential relationships between air masses and the aerosol Hg multi-isotopic compositions, we modelled daily 72 h back-trajectories at a 10 m agl height using HYSPLIT (Hybrid Single Particles Lagrangian Integrated Trajectory) for each sample. The model used NCEP-NCAR reanalysis data fields,

using a 2.5-degree latitude-longitude global grid with a time resolution of 6 h obtained from the Air Resources Laboratory (ARL). Back-trajectories were ultimately incorporated into a map generated by GMT (Generic mapping tools).

The significance of each correlation was calculated using a Spearman Correlation, as this non-parametrical test does not carry any assumption about the data distribution and is not sensitive to outliers.

3 RESULTS

Mercury multi-isotopic compositions in aerosols from stations 13 and 98 are reported in **Tables 1, 2**, respectively. For downtown station 13 ($n = 24$), $\delta^{202}\text{Hg}$ vary from -4.00 to -1.30‰ with a mean value of $-2.65 \pm 0.63\text{‰}$ (2σ), $\Delta^{199}\text{Hg}$ from -0.06 to 0.33‰ with a mean value of $0.08 \pm 0.08\text{‰}$ (2σ), $\Delta^{200}\text{Hg}$ from -0.04 to 0.07‰ with a mean value of $0.02 \pm 0.02\text{‰}$ (2σ) and $\Delta^{201}\text{Hg}$ from -0.02 to 0.32‰ with a mean-value of $0.02 \pm 0.07\text{‰}$ (2σ). For suburban station 98 ($n = 24$), $\delta^{202}\text{Hg}$ vary from -3.70 to -1.20‰ with a mean-value of $-2.46 \pm 0.56\text{‰}$ (2σ), $\Delta^{199}\text{Hg}$ from -0.07 to 0.78‰ with a mean-value of $0.14 \pm 0.22\text{‰}$ (2σ), $\Delta^{200}\text{Hg}$ from -0.04 to 0.12‰ with a mean-value of $0.03 \pm 0.04\text{‰}$ (2σ) and $\Delta^{201}\text{Hg}$ from -0.10 to 0.69‰ with a mean-value of $0.06 \pm 0.18\text{‰}$ (2σ). A comparison with the values available in the literature is provided in the **Supplementary**



Materials. Overall, the mean values for Hg isotope compositions are very close for each of the compared stations.

A locally weighted scatter plot smoothing (LOWESS) was applied to reveal seasonal variations in the Hg multi-isotopic compositions for each station (Figures 2A–D), as this non-parametric fitting provides a flexible approach to represent data without assuming the data must fit a particular type of distribution. As a result, station 98 presents a seasonality, with the highest values observed during summer for both odd (0.78% ; $\Delta^{199}\text{Hg}$ and $\Delta^{201}\text{Hg}$) and even-MIF (0.15% ; $\Delta^{200}\text{Hg}$), whereas station 13 does not present any seasonality. This suggests that distinct factors control the Hg isotope systematics at stations 13 and 98.

Besides, station 13 is characterized by higher NO_x ($\text{NO} + \text{NO}_2$) concentrations, varying from 10 to 54 ppb with a mean of 24 ± 11.8 ppb, whereas they vary from 0.8 to 54 ppb, with a mean of

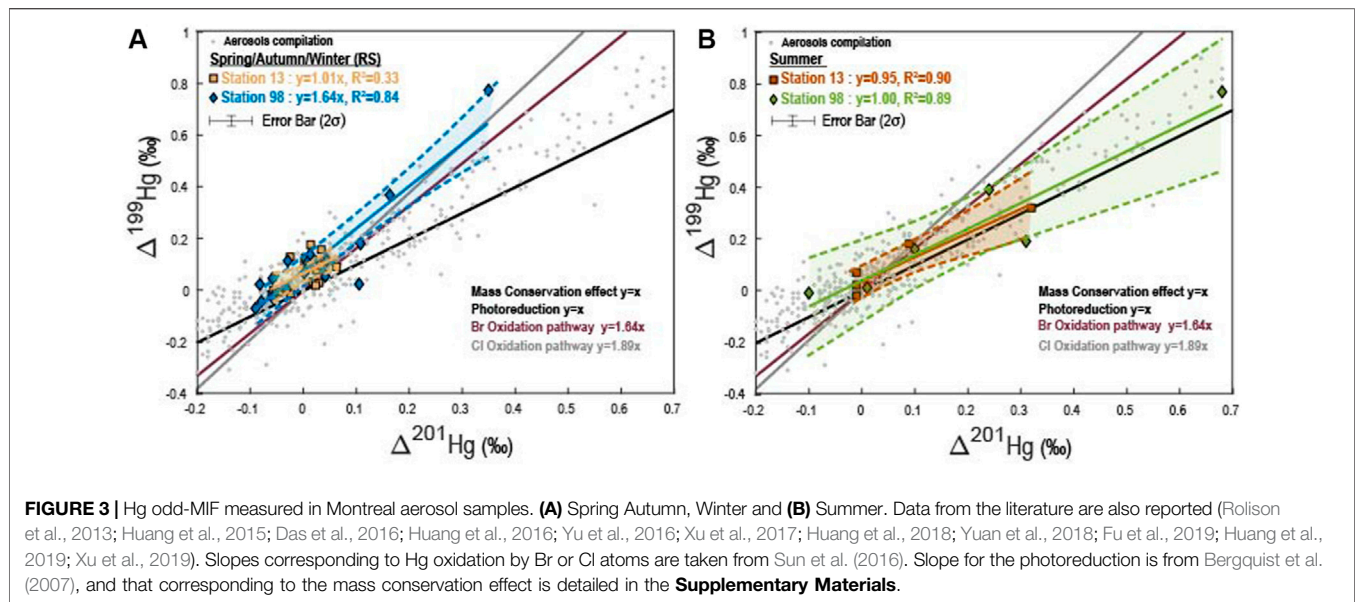
8 ± 10.8 ppb, at station 98 (Tables 1, 2). We also observe that sulfate (SO_4^{2-}) concentrations are significantly higher (p -values = 0.01) at station 13 compared to station 98, in agreement with the fact that station 13 is expected to be largely impacted by human activities (Tables 1, 2). Moreover, yearly ozone (O_3) concentrations are also significantly higher (p -values < 0.01) at station 98 compared to station 13, varying from 5 to 44 ppb with a mean concentration of 26 ± 9 ppb, and from 4 to 36 ppb with a mean concentration of 20 ± 8 ppb, respectively (Tables 1, 2).

4 DISCUSSION

The mechanisms of PBM formation are not well constrained as uncertainties remain on 1) the main Hg species (i.e., Hg^0 or Hg^{II}) that are incorporated into PBM (Seigneur, 1998; Amos et al., 2012; Kurien et al., 2017) and 2) the eventual isotopic fractionation associated to the incorporation of Hg^{II} . In the following section, we will discuss the mechanisms and the main sources responsible for the variation of Hg isotopic compositions measured on PBM at stations 13 and 98, based on our dataset and the previous experimental results from the Hg^0 oxidation and Hg^{II} photoreduction that have been widely used in the literature to address the origin and possible impact factors of PBM (Huang et al., 2015; Huang et al. 2016; Huang et al. 2018; Fu et al., 2019; Huang et al., 2019; Qiu et al., 2021).

4.1 Influence of Anthropogenic Emissions

The both low odd and even-MIF, close to 0‰, coupled to the absence of Hg isotopic seasonality at station 13, suggest that the factor controlling the Hg multi-isotopic compositions is constant and perennial during 2015. This contrasts with the seasonality in the Hg isotopic compositions previously reported in urban areas that has been demonstrated to reflect varying contributions from anthropogenic emission sources (Huang et al., 2016; Huang et al., 2018). Still, considering the geographical location of station 13, we hypothesize that the corresponding Hg isotopic compositions may be largely impacted by anthropogenic emissions. In fact, the low Hg-MIF, in particular the $\Delta^{199}\text{Hg}$ close to 0‰, and the negative $\delta^{202}\text{Hg}$ measured at this station are characterized by values that are consistent and within the range of variations reported for anthropogenic emissions (Biswas et al., 2008, Sun et al., 2014, Yin et al., 2014, Wang et al., 2015, Das et al., 2016, Huang et al., 2016, Zheng et al., 2016, Wang T. et al., 2017; Wang T. et al., 2017, Huang et al., 2018, Yuan et al., 2018, Zhang et al., 2020). Moreover, we observe that the $\Delta^{199}\text{Hg}/\Delta^{201}\text{Hg}$ ratio, a proxy for identifying processes triggering Hg-MIF (Bergquist et al., 2007; Zheng et al., 2009; Sherman et al., 2010; Sun et al., 2016) is characterized by a yearly value close to 0.95 at station 13. A $\Delta^{199}\text{Hg}/\Delta^{201}\text{Hg}$ ratio ranging from 1 to 1.3 is generally explained as the result of photoreduction (Bergquist et al., 2007; Zheng et al., 2009). As seen, Supplementary Figure S1 reports a compilation of primary aerosols emitted by various emission sources and shows that anthropogenic PBM is characterized by a $\Delta^{199}\text{Hg}/\Delta^{201}\text{Hg}$ ratio of 1.075, close to the 0.95 $\Delta^{199}\text{Hg}/\Delta^{201}\text{Hg}$ ratio we observe at station 13 (Figure 3),



implying probably a dominance of anthropogenic emissions while the implication of photoreduction cannot be rejected. Without further data, determining the respective contributions of primary (mixing) and secondary (photoreduction) Hg is difficult at this point. Moreover, as both mechanisms do not yield specific $\Delta^{200}\text{Hg}$ variation in the $\Delta^{201}\text{Hg}/\Delta^{200}\text{Hg}$ and $\Delta^{199}\text{Hg}/\Delta^{200}\text{Hg}$ diagrams (Figure 4), even-MIF cannot be used to distinguish sources from process effects (Bergquist et al., 2007; Zheng et al., 2009). The identification of the different sources involved is not further discussed here as it is beyond the scope of our study. However, in the case of a dominance of anthropogenic emission, we suggest that the anthropogenic sources and their respective contributions are not expected to vary over time, as demonstrated by the absence of Hg isotope seasonality at station 13.

Unlike at station 13, samples collected at station 98 display a seasonality in their Hg isotopic compositions, with positive peaks for both odd- and even-MIF in the summer, with values up to 0.78 and 0.15‰, respectively. As the range of Hg concentrations at stations 98 and 13 are similar (i.e., varying from ~30 to 1800 ng m⁻³), this suggests that, in addition to anthropogenic inputs, the Hg isotopic compositions of aerosols at station 98 may be modified by secondary processes.

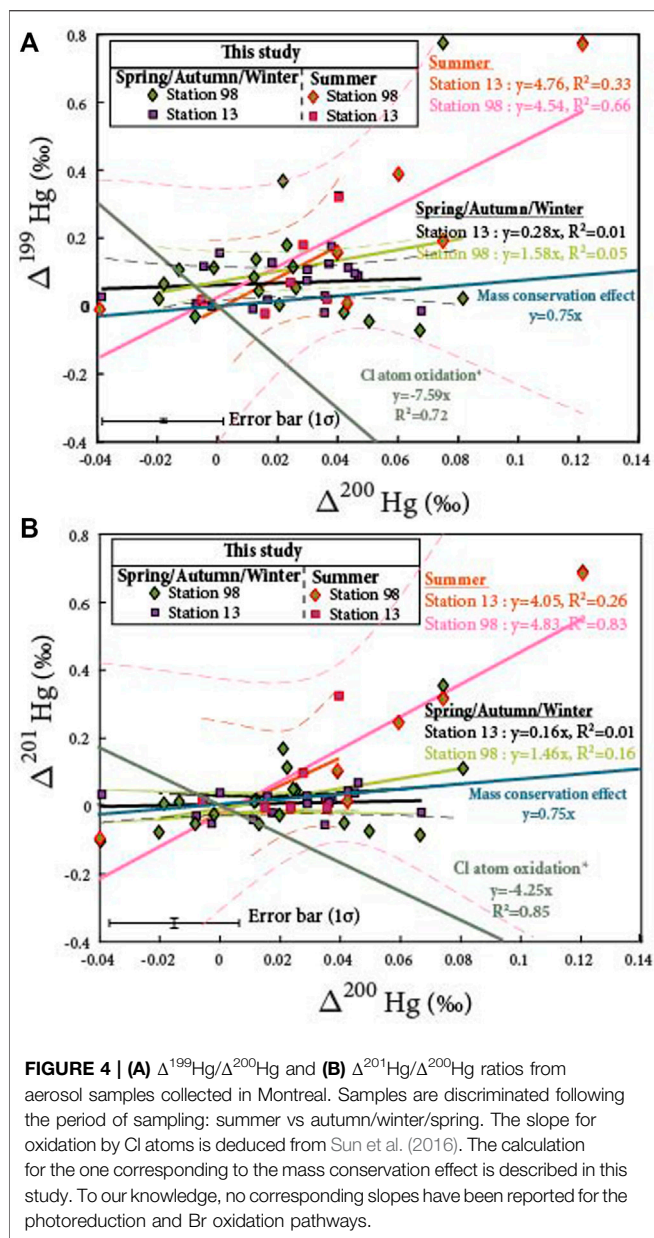
4.2 Secondary Processes That May Impact Atmospheric Hg Isotope Signatures

The annual seasonality for the $\delta^{202}\text{Hg}$ and odd-MIF we observe at station 98 presents similarities with the one reported by Huang et al. (2018) in the urban area of Xiamen (China) where the authors measured low $\delta^{202}\text{Hg}$ (i.e., down to -4‰) in winter and high $\Delta^{199}\text{Hg}$, up to 0.7‰ in summer. This is also in agreement with the $\Delta^{199}\text{Hg}$ seasonality reported by Huang et al. (2016) in the urban area of Beijing that also presents the highest values in summer but differences in the $\delta^{202}\text{Hg}$ seasonality with the

corresponding highest values measured during the winter. Finally, our findings are also consistent with the seasonality reported by Fu et al. (2019) in a forested site with high $\Delta^{199}\text{Hg}$ -values, up to 0.82‰, in the summer. The authors explained the seasonality by either varying contributions from Hg sources, in particular local anthropogenic ones, or by the long-distance transportation of atmospheric Hg (Huang et al., 2018; Fu et al., 2019). In order to better constrain the potential mechanisms triggering the seasonal variations of Hg isotope MIF, we elected to separate our results obtained at station 98 into two periods, the summer (i.e., high Hg-MIF) and the remaining seasons (i.e., spring, autumn and winter, thereafter referred as RS). This discrimination is based on the fact that PBM samples during these two periods present distinct Hg isotopic compositions, with a mean $\Delta^{199}\text{Hg}/\Delta^{201}\text{Hg}$ ratio of 1.63 ($R^2 = 0.84$, p -value < 0.01) for RS aerosols and of 1 ($R^2 = 0.89$, p -value = 0.02) for summer ones.

4.2.1 Tropospheric Hg⁰ Oxidation by Halogen Atoms

Coupled to the experimental results reported by previous studies (Bergquist et al., 2007; Zheng et al., 2009; Sun et al., 2016), we may explain the $\Delta^{199}\text{Hg}/\Delta^{201}\text{Hg}$ ratio of 1.63 we observed for aerosol samples collected during spring, autumn, and winter at station 98 by a two-steps mixing between 1) Hg^{II} derived from the oxidation of Hg⁰ by halogen atoms (i.e., Br and Cl) that isotopically fractionates Hg isotopes with typical $\Delta^{199}\text{Hg}/\Delta^{201}\text{Hg}$ ratios of 1.63 (Br⁻) or 1.89 (Cl⁻) (Sun et al., 2016), with 2) either primary anthropogenic emissions (see above) or Hg that has undergone photoreduction that will introduce a typical $\Delta^{199}\text{Hg}/\Delta^{201}\text{Hg}$ ratio varying from 1 to 1.3 for the residual Hg^{II} (Bergquist et al., 2007; Zheng et al., 2009). Such mixing will produce Hg with an intermediate $\Delta^{199}\text{Hg}/\Delta^{201}\text{Hg}$ ratio varying from 1 to 1.89, which would be consistent with the $\Delta^{199}\text{Hg}/\Delta^{201}\text{Hg}$ ratio of 1.63 that we observed. Furthermore, this high 1.63 ratio suggests that PBM measured during the RS period would be



mostly dominated by Hg^{II} formed by the oxidation of Hg^0 by halogen atoms, and that the contributions from photoreduction and/or anthropogenic emissions would thus be less impactful. The PBM measured during the RS period is also characterized by Hg isotopic compositions that do not follow any trend in both the $\Delta^{199}\text{Hg}/\Delta^{200}\text{Hg}$ ($R^2 = 0.05$, p -value = 0.74) and $\Delta^{201}\text{Hg}/\Delta^{200}\text{Hg}$ ($R^2 = 0.16$, p -value = 0.26) diagrams. This absence of trends between the odd-MIF and the even-MIF may either reflect that Br oxidation (Sun et al., 2016), Hg photoreduction (Bergquist et al., 2007; Zheng et al., 2009) and of anthropogenic emissions (Supplementary Figure S1) are involved, suggesting the probable contribution of the latest to the atmospheric PBM in Montreal. However, considering that station 98 is less exposed to anthropogenic emissions (Boulet and Melancon, 2011) as it is also

illustrated by the higher concentration of NO_x in the station 13 than in station 98 (i.e., a mean concentration value of 24 ± 11.8 ppb vs a mean concentration value of 8 ± 10.8 ppb, respectively), we can then hypothesize that the Hg isotopic compositions measured during the RS period mainly reflect successive oxidation and photoreduction reactions.

4.2.2 Additional Factors Controlling Hg Isotopes in Summer

Summer PBM samples measured at station 98 display Hg isotopic compositions distinct from the RS ones, with a $\Delta^{199}\text{Hg}/\Delta^{201}\text{Hg}$ ratio of 1.00 ($R^2 = 0.89$; Figure 3), a $\Delta^{201}\text{Hg}/\Delta^{200}\text{Hg}$ ratio of 4.83 ($R^2 = 0.83$), and a $\Delta^{199}\text{Hg}/\Delta^{200}\text{Hg}$ ratio of 4.54 ($R^2 = 0.66$; Figures 4A,B). Similarly to station 13, while a $\Delta^{199}\text{Hg}/\Delta^{201}\text{Hg}$ ratio of 1.00 may result from photoreduction and/or anthropogenic inputs, these two processes cannot explain neither the high $\Delta^{200}\text{Hg}$ values, up to 0.15‰, nor the $\Delta^{201}\text{Hg}/\Delta^{200}\text{Hg}$ ratio of 4.83. This suggests that at least one other process and/or source must be involved. The different hypotheses regarding their characteristics are discussed below.

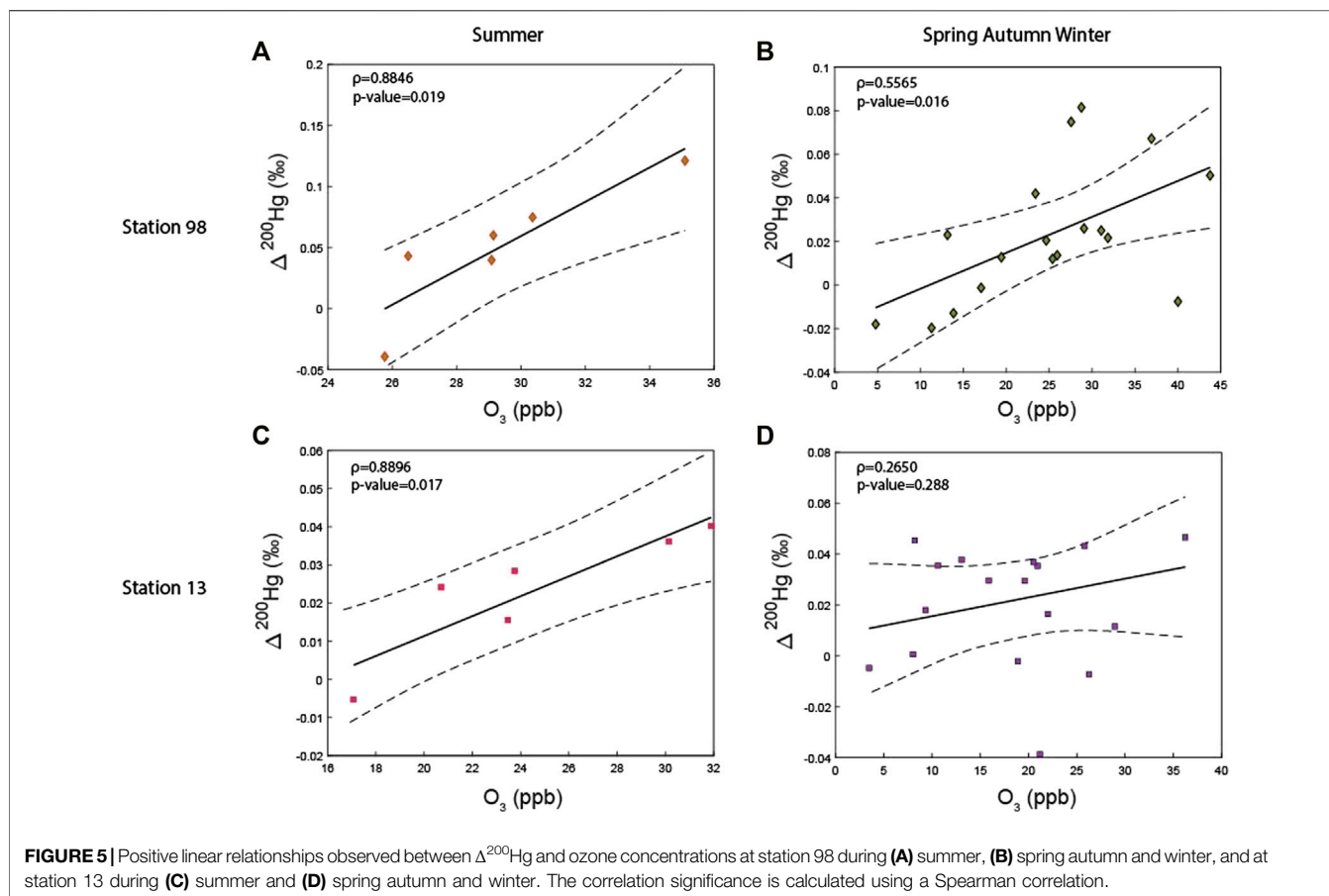
4.2.2.1. Stratospheric Inputs

Positive $\Delta^{200}\text{Hg}$ have been reported in PBM and precipitation worldwide, though the mechanisms triggering such even-MIF remain unclear (Gratz et al., 2010; Chen et al., 2012; Demers et al., 2013; Rolison et al., 2013; Demers et al., 2015). Positive $\Delta^{200}\text{Hg}$ anomalies in atmospheric samples have been suggested to result from the photochemical oxidation of Hg^0 in the upper troposphere and/or stratosphere (Chen et al., 2012). The hypothesis of a stratospheric input would also account for the positive odd-Hg MIF considering 1) the hypothesis made by Fu et al. (2019) that the photoreduction of aerosols fractionate Hg isotopes in a similar way to photoreduction in aqueous solutions and 2) that Hg photoreduction in the stratosphere would occur at a higher magnitude than in the troposphere as more UV irradiations (and wavelengths) are available in the stratosphere (Molina et al., 1986).

To test this hypothesis, we used HYSPLIT to simulate a 3-days back-trajectories for each of our sample. We observed that none of our summer aerosol samples reached an altitude higher than 2000 m (Supplementary Figure S2). Furthermore, the stratosphere-troposphere exchange (STE) in the Northern Hemisphere close to Montreal is preferentially located in the Northern Pacific and Northern Atlantic (Sprenger and Wernli, 2003; Gettelman et al., 2011; Boothe et al., 2017) and presents higher mass fluxes during the winter than in the summer (i.e., $\sim 250 \text{ kg s}^{-1} \text{ km}^{-2}$ vs $\sim 100 \text{ kg s}^{-1} \text{ km}^{-2}$, respectively; Boothe et al. (2017)). Thus, as demonstrated by Chen et al. (2012), $\Delta^{200}\text{Hg}$ would be more positive in winter than in summer, which is not what we have been observed. Ultimately, our results demonstrate that a contribution of stratospheric Hg is highly unlikely, implying that this cannot explain the positive $\Delta^{200}\text{Hg}$ we measured during the summer.

4.2.2.2. The Mass Conservation Effect

Farquhar et al. (2007) discussed the mass conservation effect and demonstrated that this process can generate small MIF, even at



equilibrium after mixing. The mass conservation effect has also been shown to play a role in the variations of the S multi-isotopic compositions in metabolic and biogeochemical networks (Farquhar et al., 2007). We suggest that these small MIF would also occur for Hg isotopes and produce distinct $\Delta^{199}\text{Hg}/\Delta^{201}\text{Hg}$, $\Delta^{201}\text{Hg}/\Delta^{200}\text{Hg}$ and $\Delta^{199}\text{Hg}/\Delta^{200}\text{Hg}$ ratios of 1.01, 0.74, and 0.75, respectively (see **Supplementary Materials** for more details). Although the $\Delta^{199}\text{Hg}/\Delta^{201}\text{Hg}$ ratio of 1.0 measured at station 98 during the summer yields a value consistent with the one characterizing this mass conservation effect, the corresponding $\Delta^{201}\text{Hg}/\Delta^{200}\text{Hg}$ (4.83) and $\Delta^{199}\text{Hg}/\Delta^{200}\text{Hg}$ (4.54) ratios cannot be explained by this effect. It follows that the mass conservation effect is unlikely responsible for the high $\Delta^{199}\text{Hg}$ and $\Delta^{200}\text{Hg}$ values, of up to 0.78 and 0.15‰, that we measured during summer.

4.2.2.3. Additional Oxidation Process Involved

Since none of the aforementioned reactions can explain the high $\Delta^{199}\text{Hg}$ and $\Delta^{200}\text{Hg}$ measured in the summer PBM at station 98, we suggest that an alternative additional reaction must be involved. We observed that $\Delta^{200}\text{Hg}$ is strongly correlated to ozone (O_3) concentrations at station 98, both during the summer (p -value = 0.02) and the RS (p -value = 0.02) periods (**Figure 5**). This underlines the possibility of a reaction involving O_3 . The Hg oxidation by ozone (O_3) has actually been identified

as a potential pathway to convert atmospheric Hg^0 (and Hg^{I}) into reactive gas Hg^{II} (RGM) that may ultimately be incorporated into aerosols, thus contributing to the Hg atmospheric budget (De Simone et al., 2015; Travnikov et al., 2017). Although theoretical doubts remain about its viability and significance for the oxidation of Hg^0 (Calvert et al., 2005), a recent study suggested that O_3 could be the main oxidant of Hg^{I} (Shah et al., 2021). Our hypothesis would also be consistent with the findings of Ren et al. (2014) who highlighted a positive correlation between the concentrations of gaseous oxidized mercury (GOM) and O_3 in the Northern Gulf of Mexico. Thus, to our knowledge, this study is the first to highlight a correlation between the ozone concentration and the even-MIF, bringing thus an additional argument that O_3 might be involved in Hg^0 oxidation.

Still, the variations of the Hg multi-isotopic compositions measured at station 98 may reflect, at least partially, a seasonal transition from the tropospheric Hg^0 oxidation by halogen radicals, from autumn to spring, to an oxidation by ozone process during the summer. This hypothesis is consistent with the fact that tropospheric reactive halogens radicals (Cl, Br or I) have been shown to play an important role in the ozone cycle by destroying O_3 through catalytic cycles (Chameides et al., 1980) and by decreasing its production rate (Von Glasow et al., 2004). It comes that when halogen atoms are dominating during the RS period, they will represent the major oxidant reservoir for Hg^0 . In

contrast, during summer, ozone becomes the dominating source of Hg^0 oxidants as its concentrations become higher due to a higher influence of solar radiations during that period. This scenario is also consistent with the findings of Shah et al. (2021) who demonstrated that the two main oxidation pathways involving halogen atoms, OH and ozone can coexist. Besides, concentrations of atmospheric reactive halogens that are of marine origin have been extensively reported to decrease during the summer (Keene et al., 2007; Gao et al., 2010), leaving room for the ozone concentrations to increase during that period. This emphasizes the importance in future studies of 1) measuring the concentration of halogen atoms and 2) determining the source of halogen atoms at stations 13 and 98, in order to verify our hypothesis. Furthermore, future experimental studies are still needed to specifically characterize the Hg multi-isotopic fractionations associated to this O_3 oxidation pathway. In that perspective and to account for the Hg isotopic compositions we measured in Montreal, we predict that O_3 oxidation should fractionate Hg isotopes following a $\Delta^{199}\text{Hg}/\Delta^{201}\text{Hg}$ ratio of ~ 1 and $\Delta^{199}\text{Hg}/\Delta^{200}\text{Hg}$ and $\Delta^{201}\text{Hg}/\Delta^{200}\text{Hg}$ ratios both close to 4.5.

4.3 Implications and Conclusion

Our study demonstrates that the current scheme for atmospheric Hg that only considers anthropogenic emissions, oxidation by halogen atoms and photoreduction cannot account for the whole range of Hg multi-isotopic compositions we measured in atmospheric PBM in Montreal. Based on the strong correlations we observe between $\Delta^{200}\text{Hg}$ and the ozone concentrations, we suggest that Hg oxidation involving ozone might represent the missing oxidation pathway. Our results also demonstrate that an approach coupling Hg isotopic compositions and chemistry discriminates the different oxidation mechanisms controlling the Hg atmospheric budget. Indeed, as both odd and even-MIF Hg isotopic compositions cannot be explained by halogen atom oxidation pathways, nor anthropogenic emissions, nor stratospheric inputs, this demonstrates the necessity that another oxidation pathway is involved. In that perspective, integrating the Hg oxidation by O_3 in the current atmospheric models would help better elucidate the Hg biogeochemical cycle, both in distinct environments and during different seasons, in particular in industrialized urban areas where high O_3 concentrations resulting from the photochemical oxidation of VOCs and CO in the presence of nitrogen oxides (NO_x) have been reported. These urban precursors (i.e., VOCs, CO, and NO_x) concentrations are higher in industrialized urban areas compared to sub-rural and urban ones (Jia et al., 2008). They are mainly emitted by industrial activities, power plants and road traffic (Li et al., 2017; Zheng et al., 2018; Wang et al., 2019), in particular in emerging countries such as China that has now become a hot spot for urban pollution by ozone (Wang et al., 2017; Lu et al., 2018). Considering that O_3 oxidation would be more important in regions characterized by high O_3 concentrations, Hg^{II} and PBM concentrations should be

expected to be enhanced in these regions due to this oxidation pathways for Hg coming from non-point sources (Rutter et al., 2008), affecting Hg^{II} deposition rates and ultimately Hg^{II} fluxes at a global scale. This increase would be thus different from the increase of Hg^{II} and PBM observed due to an artifact of sampling as shown by Lynam et al. (2005). Our hypothesis is furthermore supported by the fact that Hg^0 oxidation by O_3 can exist in the presence of aerosols and is enhanced in areas experiencing high NO_2 concentrations (Hong et al., 2016; Gencarelli et al., 2017; Travnikov et al., 2017). As several model studies have shown discrepancies between observed and simulated Hg^{II} concentrations, this arises the urgent need to take both the O_3 and halogen atom oxidation pathways into account in future atmospheric models (Wang et al., 2018).

Overall, our study demonstrates that the Hg multiple isotopic compositions provide a reliable complementary proxy of the atmosphere oxidant capacity and of its chemistry that could help improve our understanding of the processes involved (Fu et al., 2019; Huang et al., 2019). Still, in order to validate our hypothesis and its significant role in the global Hg cycle, further experimental studies are needed to better understand the Hg isotopic fractionations associated to the Hg^0 oxidation by ozone.

DATA AVAILABILITY STATEMENT

The original contributions presented in the study are included in the article/**Supplementary Material**, further inquiries can be directed to the corresponding authors.

AUTHOR CONTRIBUTIONS

DAY conducted both mercury isotope and chemical composition measurements under the supervision of JC. DW provided the samples. DAY, JC, ZW, and DW interpreted the data. DAY wrote the paper with contributions from all the coauthors.

FUNDING

This study was supported by The National Natural Science Foundation of China (Nos. 41830647, 41625012, 41961144028, U1612442) to JC, and the Chinese Academy of Science President's International Fellowship Initiative (PIFI-C, Grant 2018PC0034) to DAY.

SUPPLEMENTARY MATERIAL

The Supplementary Material for this article can be found online at: <https://www.frontiersin.org/articles/10.3389/fenvs.2021.773327/full#supplementary-material>

REFERENCES

- Amos, H. M., Jacob, D. J., Holmes, C. D., and Fisher, J. A. (2012). Gas-particle Partitioning of Atmospheric Hg (II) and its Effect on Global Mercury Deposition. *Atmos. Chem. Phys.* 12, 4. doi:10.5194/acp-12-591-2012
- Bergquist, B. A., and Blum, J. D. (2007). Mass-Dependent and -Independent Fractionation of Hg Isotopes by Photoreduction in Aquatic Systems. *Science* 318 (5849), 417–420. doi:10.1126/science.1148050
- Biswas, A., Blum, J. D., Bergquist, B. A., Keeler, G. J., and Xie, Z. (2008). Natural Mercury Isotope Variation in Coal Deposits and Organic Soils. *Environ. Sci. Technol.* 42 (22), 8303–8309. doi:10.1021/es801444b
- Blum, J. D., and Bergquist, B. A. (2007). Reporting of Variations in the Natural Isotopic Composition of Mercury. *Anal. Bioanal. Chem.* 388 (2), 353–359. doi:10.1007/s00216-007-1236-9
- Boothe, A. C., and Homeyer, C. R. (2017). Global Large-Scale Stratosphere-Troposphere Exchange in Modern Reanalyses. *Atmos. Chem. Phys.* 17 (9), 5537–5559. doi:10.5194/acp-17-5537-2017
- Boulet, D., and Melancon, S. (2011). “Bilan environnemental. Qualité de l’air à Montréal,” in *Rapport Annuel 2011. Ville de Montréal, Service des infrastructures, du transport et de l’environnement, Direction de l’environnement et du développement durable, Division de la planification et du suivi environnemental* (Montreal: RSQA), 8.
- Boulet, D., and Melancon, S. (2013). “Bilan environnemental. Qualité de l’air à Montréal,” in *Rapport Annuel 2013. Ville de Montréal, Service de l’environnement Division de la planification et du suivi environnemental* (Montreal: RSQA), 8.
- Boulet, D., and Melancon, S. (2012). “Bilan environnemental. Qualité de l’air à Montréal,” in *Rapport Annuel 2012. Ville de Montréal, Service des infrastructures, du transport et de l’environnement, Direction de l’environnement et du développement durable, Division de la planification et du suivi environnemental* (Montreal: RSQA), 8.
- Buchachenko, A. L. (2013). Mass-independent Isotope Effects. *J. Phys. Chem. B* 117 (8), 2231–2238. doi:10.1021/jp308727w
- Cai, H., and Chen, J. (2016). Mass-independent Fractionation of Even Mercury Isotopes. *Sci. Bull.* 61 (2), 116–124. doi:10.1007/s11434-015-0968-8
- Calvert, J., and Lindberg, S. (2005). Mechanisms of Mercury Removal by O and OH in the Atmosphere. *Atmos. Environ.* 39 (18), 3355–3367. doi:10.1016/j.atmosenv.2005.01.055
- Chameides, W. L., and Davis, D. D. (1980). Iodine: Its Possible Role in Tropospheric Photochemistry. *J. Geophys. Res.* 85 (C12), 7383–7398. doi:10.1029/jc085ic12p07383
- Chen, J., Hintelmann, H., Feng, X., and Dimock, B. (2012). Unusual Fractionation of Both Odd and Even Mercury Isotopes in Precipitation from Peterborough, ON, Canada. *Geochimica et Cosmochimica Acta* 90, 33–46. doi:10.1016/j.gca.2012.05.005
- Chen, J., Hintelmann, H., Zheng, W., Feng, X., Cai, H., Wang, Z., et al. (2016). Isotopic Evidence for Distinct Sources of Mercury in lake Waters and Sediments. *Chem. Geology* 426, 33–44. doi:10.1016/j.chemgeo.2016.01.030
- Das, R., Wang, X., Khezri, B., and Webster, R. (2016). Mercury Isotopes of Atmospheric Particle Bound Mercury for Source Apportionment Study in Urban Kolkata, India. *Elem. Sci. Anth* 4, 1. doi:10.12952/journal.elementa.000098
- Dauphas, N., and Schauble, E. A. (2016). Mass Fractionation Laws, Mass-independent Effects, and Isotopic Anomalies. *Annu. Rev. Earth Planet. Sci.* 44, 709–783. doi:10.1146/annurev-earth-060115-012157
- De Simone, F., Cinnirella, S., Gencarelli, C. N., Yang, X., Hedgecock, I. M., and Pirrone, N. (2015). Model Study of Global Mercury Deposition from Biomass Burning. *Environ. Sci. Technol.* 49 (11), 6712–6721. doi:10.1021/acs.est.5b00969
- Demers, J. D., Blum, J. D., and Zak, D. R. (2013). Mercury Isotopes in a Forested Ecosystem: Implications for Air-Surface Exchange Dynamics and the Global Mercury Cycle. *Glob. Biogeochem. Cycles* 27 (1), 222–238. doi:10.1002/gbc.20021
- Demers, J. D., Sherman, L. S., Blum, J. D., Marsik, F. J., and Dvonch, J. T. (2015). Coupling Atmospheric Mercury Isotope Ratios and Meteorology to Identify Sources of Mercury Impacting a Coastal Urban-Industrial Region Near Pensacola, Florida, USA. *Glob. Biogeochem. Cycles* 29 (10), 1689–1705. doi:10.1002/2015gb005146
- Estrade, N., Carignan, J., Sonke, J. E., and Donard, O. F. X. (2009). Mercury Isotope Fractionation during Liquid-Vapor Evaporation Experiments. *Geochimica et Cosmochimica Acta* 73 (10), 2693–2711. doi:10.1016/j.gca.2009.01.024
- Farquhar, J., Johnston, D. T., and Wing, B. A. (2007). Implications of Conservation of Mass Effects on Mass-dependent Isotope Fractionations: Influence of Network Structure on Sulfur Isotope Phase Space of Dissimilatory Sulfate Reduction. *Geochimica et Cosmochimica Acta* 71 (24), 5862–5875. doi:10.1016/j.gca.2007.08.028
- Farquhar, J., and Wing, B. A. (2003). Multiple Sulfur Isotopes and the Evolution of the Atmosphere. *Earth Planet. Sci. Lett.* 213 (1), 1–13. doi:10.1016/s0012-821x(03)00296-6
- Fu, X., Jiskra, M., Yang, X., Maruszczak, N., Enrico, M., Chmieleff, J., et al. (2021). Mass-Independent Fractionation of Even and Odd Mercury Isotopes during Atmospheric Mercury Redox Reactions. *Environ. Sci. Technol.* 55 (14), 10164–10174. doi:10.1021/acs.est.1c02568
- Fu, X., Maruszczak, N., Wang, X., Gheusi, F., and Sonke, J. E. (2016). Isotopic Composition of Gaseous Elemental Mercury in the Free Troposphere of the Pic du Midi Observatory, France. *Environ. Sci. Technol.* 50 (11), 5641–5650. doi:10.1021/acs.est.6b00033
- Fu, X., Zhang, H., Feng, X., Tan, Q., Ming, L., Liu, C., et al. (2019). Domestic and Transboundary Sources of Atmospheric Particulate Bound Mercury in Remote Areas of China: Evidence from Mercury Isotopes. *Environ. Sci. Technol.* 53 (4), 1947–1957. doi:10.1021/acs.est.8b06736
- Gao, Y., Sun, M., Wu, X., Liu, Y., Guo, Y., and Wu, J. (2010). Concentration Characteristics of Bromine and Iodine in Aerosols in Shanghai, China. *Atmos. Environ.* 44 (34), 4298–4302. doi:10.1016/j.atmosenv.2010.05.047
- Gencarelli, C. N., Bieser, J., Carbone, F., De Simone, F., Hedgecock, I. M., Matthias, V., et al. (2017). Sensitivity Model Study of Regional Mercury Dispersion in the Atmosphere. *Atmos. Chem. Phys.* 17 (1), 627–643. doi:10.5194/acp-17-627-2017
- Geng, H., Yin, R., and Li, X. (2018). An Optimized Protocol for High Precision Measurement of Hg Isotopic Compositions in Samples with Low Concentrations of Hg Using MC-ICP-MS. *J. Anal. Spectrom.* 33 (11), 1932–1940. doi:10.1039/c8ja00255j
- Gottelman, A., Hoor, P., Pan, L. L., and Randel, W. J. (2011). The Extratropical Upper Troposphere and Lower Stratosphere. *Rev. Geophys.* 49 (3), 1. doi:10.1029/2011rg000355
- Gratz, L. E., Keeler, G. J., Blum, J. D., and Sherman, L. S. (2010). Isotopic Composition and Fractionation of Mercury in Great Lakes Precipitation and Ambient Air. *Environ. Sci. Technol.* 44 (20), 7764–7770. doi:10.1021/es100383w
- Holmes, C. D., Jacob, D. J., Corbitt, E. S., and Mao, J. (2010). Global Atmospheric Model for Mercury Including Oxidation by Bromine Atoms. *Atmos. Chem. Phys.* 10, 1. doi:10.5194/acp-10-12037-2010
- Hong, Q., Xie, Z., Liu, C., Wang, F., Xie, P., Kang, H., et al. (2016). Speciated Atmospheric Mercury on Haze and Non-haze Days in an Inland City in China. *Atmos. Chem. Phys.* 16 (21), 13807–13821. doi:10.5194/acp-16-13807-2016
- Horowitz, H. M., Jacob, D. J., Zhang, Y., Dibble, T. S., Slemr, F., Amos, H. M., et al. (2017). A New Mechanism for Atmospheric Mercury Redox Chemistry: Implications for the Global Mercury Budget. *Atmos. Chem. Phys.* 17 (10), 6353–6371. doi:10.5194/acp-17-6353-2017
- Huang, Q., Chen, J., Huang, W., Fu, P., Guinot, B., Feng, X., et al. (2016). Isotopic Composition for Source Identification of Mercury in Atmospheric fine Particles. *Atmos. Chem. Phys.* 16 (18), 11773–11786. doi:10.5194/acp-16-11773-2016
- Huang, Q., Chen, J., Huang, W., Reinfelder, J. R., Fu, P., Yuan, S., et al. (2019). Diel Variation in Mercury Stable Isotope Ratios Records Photoreduction of PM_{2.5}-bound Mercury. *Atmos. Chem. Phys.* 19 (1), 315–325. doi:10.5194/acp-19-315-2019
- Huang, Q., Liu, Y., Chen, J., Feng, X., Huang, W., Yuan, S., et al. (2015). An Improved Dual-Stage Protocol to Pre-concentrate Mercury from Airborne Particles for Precise Isotopic Measurement. *J. Anal. Spectrom.* 30 (4), 957–966. doi:10.1039/c4ja00438h
- Huang, S., Sun, L., Zhou, T., Yuan, D., Du, B., and Sun, X. (2018). Natural Stable Isotopic Compositions of Mercury in Aerosols and Wet Precipitations Around a Coal-Fired Power Plant in Xiamen, Southeast China. *Atmos. Environ.* 173, 72–80. doi:10.1016/j.atmosenv.2017.11.003
- Jia, C., Batterman, S., and Godwin, C. (2008). VOCs in Industrial, Urban and Suburban Neighborhoods, Part 1: Indoor and Outdoor Concentrations, Variation, and Risk Drivers. *Atmos. Environ.* 42 (9), 2083–2100. doi:10.1016/j.atmosenv.2007.11.055

- Keene, W. C., Stutz, J., Pszenny, A., and Maben, J. R. (2007). Inorganic Chlorine and Bromine in Coastal New England Air during Summer. *J. Geophys. Res. Atmospheres* 112 (D10), 1. doi:10.1029/2006jd007689
- Kurien, U., Hu, Z., Lee, H., Dastoor, A. P., and Ariya, P. A. (2017). Radiation Enhanced Uptake of Hg⁰(g) on Iron (Oxyhydr)oxide Nanoparticles. *RSC Adv.* 7 (71), 45010–45021. doi:10.1039/c7ra07401h
- Li, M., Zhang, Q., Kurokawa, J.-i., Woo, J.-H., He, K., Lu, Z., et al. (2017). MIX: a Mosaic Asian Anthropogenic Emission Inventory under the International Collaboration Framework of the MICS-Asia and HTAP. *Atmos. Chem. Phys.* 17 (2), 935–963. doi:10.5194/acp-17-935-2017
- Lu, X., Hong, J., Zhang, L., Cooper, O. R., Schultz, M. G., Xu, X., et al. (2018). Severe Surface Ozone Pollution in China: A Global Perspective. *Environ. Sci. Technol. Lett.* 5 (8), 487–494. doi:10.1021/acs.estlett.8b00366
- Lynam, M., and Keeler, G. (2005). Artifacts Associated with the Measurement of Particulate Mercury in an Urban Environment: The Influence of Elevated Ozone Concentrations. *Atmos. Environ.* 39 (17), 3081–3088. doi:10.1016/j.atmosenv.2005.01.036
- Mead, C., Lyons, J. R., Johnson, T. M., and Anbar, A. D. (2013). Unique Hg Stable Isotope Signatures of Compact Fluorescent Lamp-Sourced Hg. *Environ. Sci. Technol.* 47 (6), 2542–2547. doi:10.1021/es303940p
- Molina, L. T., and Molina, M. J. (1986). Absolute Absorption Cross Sections of Ozone in the 185- to 350-nm Wavelength Range. *J. Geophys. Res.* 91 (D13), 14501–14508. doi:10.1029/jd091d13p14501
- Paris, R., Desboeufs, K. V., Formenti, P., Nava, S., and Chou, C. (2010). Chemical Characterisation of Iron in Dust and Biomass Burning Aerosols during AMMA-SOP0/DABEX: Implication for Iron Solubility. *Atmos. Chem. Phys.* 10 (9), 4273–4282. doi:10.5194/acp-10-4273-2010
- Qiu, Y., Gai, P., Yue, F., Zhang, Y., He, P., Kang, H., et al. (2021). Identification of Potential Sources of Elevated PM_{2.5}-Hg Using Mercury Isotopes during Haze Events. *Atmos. Environ.* 247, 118203. doi:10.1016/j.atmosenv.2021.118203
- Ren, X., Luke, W., Kelley, P., Cohen, M., Ngan, F., Artz, R., et al. (2014). Mercury Speciation at a Coastal Site in the Northern Gulf of Mexico: Results from the Grand Bay Intensive Studies in Summer 2010 and spring 2011. *Atmosphere* 5 (2), 230–251. doi:10.3390/atmos5020230
- Rolison, J. M., Landing, W. M., Luke, W., Cohen, M., and Salters, V. J. M. (2013). Isotopic Composition of Species-specific Atmospheric Hg in a Coastal Environment. *Chem. Geology*. 336, 37–49. doi:10.1016/j.chemgeo.2012.10.007
- Rutter, A. P., Schauer, J. J., Lough, G. C., Snyder, D. C., Kolb, C. J., Von Kloooster, S., et al. (2008). A Comparison of Speciated Atmospheric Mercury at an Urban center and an Upwind Rural Location. *J. Environ. Monit.* 10 (1), 102–108. doi:10.1039/b710247j
- Saiz-Lopez, A., Sitkiewicz, S. P., Roca-Sanjuán, D., Oliva-Enrich, J. M., Dávalos, J. Z., Notario, R., et al. (2018). Photoreduction of Gaseous Oxidized Mercury Changes Global Atmospheric Mercury Speciation, Transport and Deposition. *Nat. Commun.* 9 (1), 4796. doi:10.1038/s41467-018-07075-3
- Seigneur, C. (1998). Mercury Adsorption to Elemental Carbon (Soot) Particles and Atmospheric Particulate Matter. *Atmos. Environ.* 32 (14–15), 2649–2657. doi:10.1016/s1352-2310(97)00415-9
- Selin, N. E. (2009). Global Biogeochemical Cycling of Mercury: A Review. *Annu. Rev. Environ. Resour.* 34 (1), 43–63. doi:10.1146/annurev.enviro.051308.084314
- Shah, V., Jacob, D. J., Thackray, C. P., Wang, X., Sunderland, E. M., Dibble, T. S., et al. (2021). Improved Mechanistic Model of the Atmospheric Redox Chemistry of Mercury. *Environ. Sci. Tech.* 55 (21), 14445–14456. doi:10.1021/acs.est.1c03160
- Sherman, L. S., Blum, J. D., Johnson, K. P., Keeler, G. J., Barres, J. A., and Douglas, T. A. (2010). Mass-independent Fractionation of Mercury Isotopes in Arctic Snow Driven by Sunlight. *Nat. Geosci.* 3, 173–177. doi:10.1038/ngeo758
- Si, L., and Ariya, P. (2018). Recent Advances in Atmospheric Chemistry of Mercury. *Atmosphere* 9 (2), 76. doi:10.3390/atmos9020076
- Springer, M., and Wernli, H. (2003). A Northern Hemispheric Climatology of Cross-tropopause Exchange for the ERA15 Time Period (1979–1993). *J. Geophys. Res. Atmospheres* 108 (D12). doi:10.1029/2002jd002636
- Subir, M., Ariya, P. A., and Dastoor, A. P. (2012). A Review of the Sources of Uncertainties in Atmospheric Mercury Modeling II. Mercury Surface and Heterogeneous Chemistry - A Missing Link. *Atmos. Environ.* 46, 1–10. doi:10.1016/j.atmosenv.2011.07.047
- Sun, G., Sommar, J., Feng, X., Lin, C.-J., Ge, M., Wang, W., et al. (2016). Mass-Dependent and -Independent Fractionation of Mercury Isotope during Gas-phase Oxidation of Elemental Mercury Vapor by Atomic Cl and Br. *Environ. Sci. Technol.* 50 (17), 9232–9241. doi:10.1021/acs.est.6b01668
- Sun, R., Enrico, M., Heimbürger, L.-E., Scott, C., and Sonke, J. E. (2013). A Double-Stage Tube Furnace-Acid-Trapping Protocol for the Pre-concentration of Mercury from Solid Samples for Isotopic Analysis. *Anal. Bioanal. Chem.* 405 (21), 6771–6781. doi:10.1007/s00216-013-7152-2
- Sun, R., Sonke, J. E., Heimbürger, L.-E., Belkin, H. E., Liu, G., Shome, D., et al. (2014). Mercury Stable Isotope Signatures of World Coal Deposits and Historical Coal Combustion Emissions. *Environ. Sci. Technol.* 48 (13), 7660–7668. doi:10.1021/es501208a
- Sunderland, E. M. (2007). Mercury Exposure from Domestic and Imported Estuarine and marine Fish in the U.S. Seafood Market. *Environ. Health Perspect.* 115 (2), 235–242. doi:10.1289/ehp.9377
- Travnikov, O., Angot, H., Artaxo, P., Bencardino, M., Bieser, J., D'Amore, F., et al. (2017). Multi-model Study of Mercury Dispersion in the Atmosphere: Atmospheric Processes and Model Evaluation. *Atmos. Chem. Phys.* 17 (8), 5271–5295. doi:10.5194/acp-17-5271-2017
- Von Glasow, R., von Kuhlmann, R., Lawrence, M. G., Platt, U., and Crutzen, P. J. (2004). Impact of Reactive Bromine Chemistry in the Troposphere. *Atmos. Chem. Phys.* 4 (11/12), 2481–2497. doi:10.5194/acp-4-2481-2004
- Wang, P., Chen, Y., Hu, J., Zhang, H., and Ying, Q. (2019). Source Apportionment of Summertime Ozone in China Using a Source-Oriented Chemical Transport Model. *Atmos. Environ.* 211, 79–90. doi:10.1016/j.atmosenv.2019.05.006
- Wang, T., Xue, L., Brimblecombe, P., Lam, Y. F., Li, L., and Zhang, L. (2017). Ozone Pollution in China: A Review of Concentrations, Meteorological Influences, Chemical Precursors, and Effects. *Sci. Total Environ.* 575, 1582–1596. doi:10.1016/j.scitotenv.2016.10.081
- Wang, X., Lin, C.-J., Feng, X., Yuan, W., Fu, X., Zhang, H., et al. (2018). Assessment of Regional Mercury Deposition and Emission Outflow in Mainland China. *J. Geophys. Res. Atmos.* 123 (17), 9868–9890. doi:10.1029/2018jd028350
- Wang, X., Luo, J., Yin, R., Yuan, W., Lin, C.-J., Sommar, J., et al. (2017). Using Mercury Isotopes to Understand Mercury Accumulation in the Montane Forest Floor of the Eastern Tibetan Plateau. *Environ. Sci. Technol.* 51 (2), 801–809. doi:10.1021/acs.est.6b03806
- Wang, Z., Chen, J., Feng, X., and Hintelmann, H. (2015). Mass-dependent and Mass-independent Fractionation of Mercury Isotopes in Precipitation from Guiyang SW China. *Comptes Rendus Geosci.* 347 (7), 358–367. doi:10.1016/j.crte.2015.02.006
- World Health Organization (2016). *Ambient (Outdoor) Air Quality and Health*. Geneva: WHO 1.
- Xiao, Z. F., Munthe, J., and Lindqvist, O. (1991). Sampling and Determination of Gaseous and Particulate Mercury in the Atmosphere Using Gold-Coated Denuders. *Water Air Soil Pollut.* 56 (1), 141–151. doi:10.1007/bf00342268
- Xu, H. M., Sun, R. Y., Cao, J. J., Huang, R.-J., Guinot, B., Shen, Z. X., et al. (2019). Mercury Stable Isotope Compositions of Chinese Urban fine Particulates in winter Haze Days: Implications for Hg Sources and Transformations. *Chem. Geology*. 504, 267–275. doi:10.1016/j.chemgeo.2018.11.018
- Xu, H., Sonke, J. E., Guinot, B., Fu, X., Sun, R., Lanzanova, A., et al. (2017). Seasonal and Annual Variations in Atmospheric Hg and Pb Isotopes in Xi'an, China. *Environ. Sci. Technol.* 51 (7), 3759–3766. doi:10.1021/acs.est.6b06145
- Yin, R., Feng, X., and Chen, J. (2014). Mercury Stable Isotopic Compositions in Coals from Major Coal Producing Fields in China and Their Geochemical and Environmental Implications. *Environ. Sci. Technol.* 48 (10), 5565–5574. doi:10.1021/es500322n
- Yin, R., Krabbenhoft, D. P., Bergquist, B. A., Zheng, W., Lepak, R. F., and Hurley, J. P. (2016). Effects of Mercury and Thallium Concentrations on High Precision Determination of Mercury Isotopic Composition by Neptune Plus Multiple Collector Inductively Coupled Plasma Mass Spectrometry. *J. Anal. Spectrom.* 31 (10), 2060–2068. doi:10.1039/c6ja00107f
- Young, E. D., Galy, A., and Nagahara, H. (2002). Kinetic and Equilibrium Mass-dependent Isotope Fractionation Laws in Nature and Their Geochemical and Cosmochemical Significance. *Geochimica et Cosmochimica Acta* 66 (6), 1095–1104. doi:10.1016/s0016-7037(01)00832-8
- Yu, B., Fu, X., Yin, R., Zhang, H., Wang, X., Lin, C.-J., et al. (2016). Isotopic Composition of Atmospheric Mercury in China: New Evidence for Sources and Transformation Processes in Air and in Vegetation. *Environ. Sci. Technol.* 50 (17), 9262–9269. doi:10.1021/acs.est.6b01782
- Yuan, S., Chen, J., Cai, H., Yuan, W., Wang, Z., Huang, Q., et al. (2018). Sequential Samples Reveal Significant Variation of Mercury Isotope Ratios during Single

- Rainfall Events. *Sci. total Environ.* 624, 133–144. doi:10.1016/j.scitotenv.2017.12.082
- Yuan, S., Zhang, Y., Chen, J., Kang, S., Zhang, J., Feng, X., et al. (2015). Large Variation of Mercury Isotope Composition during a Single Precipitation Event at Lhasa City, Tibetan Plateau, China. *Proced. Earth Planet. Sci.* 13, 282–286. doi:10.1016/j.proeps.2015.07.066
- Zhang, Y., Chen, J., Zheng, W., Sun, R., Yuan, S., Cai, H., et al. (2020). Mercury Isotope Compositions in Large Anthropogenically Impacted Pearl River, South China. *Ecotoxicology Environ. Saf.* 191, 110229. doi:10.1016/j.ecoenv.2020.110229
- Zheng, B., Tong, D., Li, M., Liu, F., Hong, C., Geng, G., et al. (2018). Trends in China's Anthropogenic Emissions since 2010 as the Consequence of Clean Air Actions. *Atmos. Chem. Phys.* 18 (19), 14095–14111. doi:10.5194/acp-18-14095-2018
- Zheng, W., and Hintelmann, H. (2010). Isotope Fractionation of Mercury during its Photochemical Reduction by Low-Molecular-Weight Organic Compounds. *J. Phys. Chem. A.* 114 (12), 4246–4253. doi:10.1021/jp9111348
- Zheng, W., and Hintelmann, H. (2009). Mercury Isotope Fractionation during Photoreduction in Natural Water Is Controlled by its Hg/DOC Ratio. *Geochimica et Cosmochimica Acta* 73 (22), 6704–6715. doi:10.1016/j.gca.2009.08.016
- Zheng, W., Obrist, D., Weis, D., and Bergquist, B. A. (2016). Mercury Isotope Compositions across North American Forests. *Glob. Biogeochem. Cycles* 30 (10), 1475–1492. doi:10.1002/2015gb005323
- Conflict of Interest:** The authors declare that the research was conducted in the absence of any commercial or financial relationships that could be construed as a potential conflict of interest.
- Publisher's Note:** All claims expressed in this article are solely those of the authors and do not necessarily represent those of their affiliated organizations, or those of the publisher, the editors and the reviewers. Any product that may be evaluated in this article, or claim that may be made by its manufacturer, is not guaranteed or endorsed by the publisher.
- Copyright © 2022 AuYang, Chen, Zheng, Lang, Wang, Wang, Zhang, Liu, Zhang, Cai, Yuan and Widory. This is an open-access article distributed under the terms of the Creative Commons Attribution License (CC BY). The use, distribution or reproduction in other forums is permitted, provided the original author(s) and the copyright owner(s) are credited and that the original publication in this journal is cited, in accordance with accepted academic practice. No use, distribution or reproduction is permitted which does not comply with these terms.